Viscoplastic squeeze flow between two identical infinite circular cylinders

A. R. Koblitz,[1,*] S. Lovett,[2] and N. Nikiforakis[1]
[1]*Department of Physics, Cavendish Laboratory, J J Thomson Avenue, Cambridge, CB3 0HE, United Kingdom*
[2]*Schlumberger Gould Research Centre, High Cross, Madingley Road, Cambridge CB3 0EL, United Kingdom*

(Received 11 October 2017; published 28 February 2018)

Direct numerical simulations of closely interacting infinite circular cylinders in a Bingham fluid are presented, and results compared to asymptotic solutions based on lubrication theory in the gap. Unlike for a Newtonian fluid, the macroscopic flow outside of the gap between the cylinders is shown to have a large effect on the pressure profile within the gap and the resulting lubrication force on the cylinders. The presented results indicate that the asymptotic lubrication solution can be used to predict the lubrication pressure only if the surrounding viscoplastic matrix is yielded by a macroscopic flow. This has implications for the use of subgrid-scale lubrication models in simulations of noncolloidal particulate suspensions in viscoplastic fluids.

DOI: 10.1103/PhysRevFluids.3.023301

I. INTRODUCTION

Complex fluids are ubiquitous in natural and industrial processes, from food processing, to lava or debris flows, to oil and gas applications. The mechanical behavior of these fluids arises from the microstructure of the fluid, for example, emulsion droplets and clays in drilling muds or polymer chains in viscoelastic fluids. When noncolloidal particles much larger than the fluid microstructure are added, the system can be thought of as a particulate suspension in a complex (continuum) fluid. Examples of these types of systems include fresh concrete and debris flows [1]. The hydrodynamic interaction between particles affects the suspension bulk properties and dynamics and is of great interest. In the case of a Newtonian fluid, analytical solutions exist for slow flow past spheres and cylinders [2,3] and the squeeze flow between them using asymptotic analysis. Viscoplastic fluids, of interest to this work, are characterized by a discontinuous nonlinear constitutive equation thereby introducing additional complexities when analytical solutions are sought.

So far, studies on interacting spheres and cylinders in viscoplastic flows have largely focused on drag and pressure drop (in the case of flow past arrays) of collinear arrangements, aligned either parallel or perpendicular to the flow [4–10]. Numerical studies using the Bingham constitutive law have been found to be in good agreement with experimental work using Carbopol 940 gels, developing drag correlations and stability criteria (with respect to sedimentation) [4,7,9,10]. Viscoplastic squeeze flow between coaxial cylindrical disks has been studied analytically for both planar [11] and axisymmetric [12,13] configurations. The configuration of collinearly approaching bodies in a viscoplastic flow has received only cursory attention in numerical studies, e.g., Refs. [8,9], with no examination of the interstitial squeeze flow.

This study therefore examines the two-dimensional squeeze flow between two approaching infinite circular cylinders in a Bingham viscoplastic fluid by direct numerical simulation. The configuration studied is such that the gap between the two cylinders is small (1% of the cylinder radius). We also make use of the asymptotic analysis by Balmforth [14] to compute leading order lubrication

*ark44@cam.ac.uk

solutions for the squeeze flow between two approaching cylinders in a Bingham fluid. We compare the analytical and numerical solutions and demonstrate that in a quasiunconfined system the squeeze flow is greatly affected by flow external to the gap, but that the asymptotic solution may be recovered under certain flow conditions in the wider domain. This is contrary to the Newtonian equivalent and has implications on using the viscoplastic lubrication force approximation as a subgrid-scale model in coarse simulation techniques.

The paper is organized as follows. In Sec. II we present the problem of interest and briefly describe the solution strategy employed for the direct numerical simulations and the lubrication theory calculations. In Sec. III we present direct numerical simulations of the quasiunconfined system. These are compared to simulations of the domain restricted to the gap only and to the asymptotic solutions from lubrication theory. These comparisons demonstrate the influence of the wider flow field on the lubrication pressure. In Sec. IV we discuss the results and the implications for subgrid-scale modeling.

II. MATHEMATICAL FORMULATION AND SOLUTION

We consider the slow, steady flow of an incompressible viscoplastic fluid around two rigid, infinite circular cylinders. The fluid has velocity $\hat{\boldsymbol{u}}(\hat{\boldsymbol{x}})$, pressure $\hat{p}(\hat{\boldsymbol{x}})$, and a symmetric total stress tensor $\hat{\boldsymbol{\tau}} - \hat{p}\boldsymbol{\delta}$, where variables with a hat are dimensional. In the absence of inertia, the conservation of mass is

$$\frac{\partial \hat{u}}{\partial \hat{x}} + \frac{\partial \hat{v}}{\partial \hat{y}} = 0, \tag{1}$$

and the conservation of momentum is

$$\frac{\partial \hat{\tau}_{xx}}{\partial \hat{x}} + \frac{\partial \hat{\tau}_{xy}}{\partial \hat{y}} - \frac{\partial \hat{p}}{\partial \hat{x}} = 0, \tag{2}$$

$$\frac{\partial \hat{\tau}_{yx}}{\partial \hat{x}} + \frac{\partial \hat{\tau}_{yy}}{\partial \hat{y}} - \frac{\partial \hat{p}}{\partial \hat{y}} = 0. \tag{3}$$

As a constitutive law we use the Bingham model

$$\begin{aligned} \hat{\tau}_{ij} &= \left(2\hat{\eta} + \frac{\hat{\tau}_Y}{\hat{\dot{\gamma}}}\right)\hat{\dot{\gamma}}_{ij} \quad \text{if } \hat{\tau} > \hat{\tau}_Y, \\ \hat{\dot{\gamma}}_{ij} &= 0 \qquad\qquad\qquad\quad \text{if } \hat{\tau} \leqslant \hat{\tau}_Y, \end{aligned} \tag{4}$$

where $\hat{\tau}_Y$ and $\hat{\eta}$ are the yield stress and the plastic viscosity of the fluid, respectively, $\hat{\dot{\gamma}}_{ij}$ is the rate of strain tensor associated with the velocity field, and

$$\hat{\dot{\gamma}}_{ij} = \frac{1}{2}\left(\frac{\partial \hat{u}_i}{\partial \hat{x}_j} + \frac{\partial \hat{u}_j}{\partial \hat{x}_i}\right), \quad \hat{\dot{\gamma}} = \sqrt{\frac{1}{2}\hat{\dot{\gamma}}_{ij}\hat{\dot{\gamma}}_{ij}}, \quad \hat{\tau} = \sqrt{\frac{1}{2}\hat{\tau}_{ij}\hat{\tau}_{ij}}. \tag{5}$$

The problem geometries are depicted in Fig. 1, where the inset highlights the portion of the system considered in the analytical investigation. Aligning the system midplane in a Cartesian coordinate system the two cylinders are placed with their centers located at $(-H/2 - D/2,0)$ and $(H/2 + D/2,0)$, where H is the minimum separation distance and D the cylinder diameter. The computational domain for the whole system has dimensions $10\,D \times 5\,D$, which is sufficiently large for the cylinders to be essentially unconfined: waning stresses away from the moving cylinders lead to the formation of a yield envelope in the immediate vicinity of the cylinders, outside of which the fluid forms a rigid plug attached to the domain walls. Because the fluid in the far field is unyielded for the range of yield stresses explored in this study, we set no-slip boundaries at $y \pm 2.5\,D$ and pressure inlets and outlets at $x \pm 5\,D$. The cylinders have a constant relative approach velocity of V.

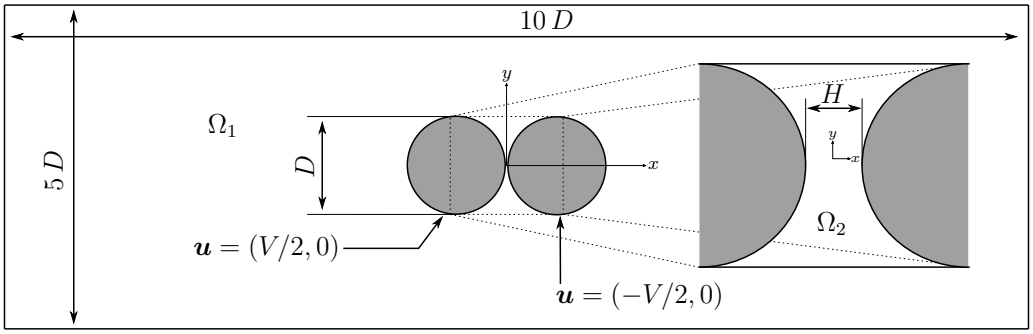

FIG. 1. Schematic showing the problem geometry for the entire flow system (Ω_1) investigated through numerical methods and the reduced system (Ω_2) investigated with both analytical and numerical methods.

A. Large-scale nondimensionalization

Choosing a velocity scale of V, length scale of D, shear rate scale of V/D, and stress scale of $\hat{\eta}V/D$, we obtain the dimensionless equations

$$\frac{\partial u}{\partial x} + \frac{\partial v}{\partial y} = 0, \tag{6}$$

$$\frac{\partial \tau_{xx}}{\partial x} + \frac{\partial \tau_{xy}}{\partial y} - \frac{\partial p}{\partial x} = 0, \tag{7}$$

$$\frac{\partial \tau_{yx}}{\partial x} + \frac{\partial \tau_{yy}}{\partial y} - \frac{\partial p}{\partial y} = 0, \tag{8}$$

$$\begin{aligned} \tau_{ij} &= \left(2 + \frac{\mathrm{Bn}}{\dot{\gamma}}\right)\dot{\gamma}_{ij} \quad \text{if } \tau > \mathrm{Bn}, \\ \dot{\gamma}_{ij} &= 0 \qquad\qquad\quad \text{if } \tau \leqslant \mathrm{Bn}, \end{aligned} \tag{9}$$

where

$$\mathrm{Bn} := \frac{\hat{\tau}_Y D}{\hat{\eta} V} \tag{10}$$

is a Bingham number for the macroscopic flow external to the gap.

B. Computational method

We numerically compute the solution of equations (6)–(9) for two approaching cylinders with a small gap size ($H/R = 0.01$ where $R \equiv D/2$ is the cylinder radius), and calculate the resulting forces on the cylinders. To handle the disparate length scales of this problem in a computationally efficient manner we use the method of overset grids (also called overlapping, overlaid or Chimera grids) in a finite difference framework to discretize the domain. This method and grid generation algorithm is discussed in detail in Chesshire and Henshaw [15], Henshaw [16], and Koblitz *et al.* [17], where its efficacy for particulate flow simulations was demonstrated. Briefly, the overset grid method represents a complex domain using multiple body-fitted curvilinear grids that are allowed to overlap while being logically rectangular. The overlapping aspect brings flexibility and efficiency to grid generation, which is beneficial for moving body problems. Here, since the cylinders are static, the chief benefit of the overset grid method is that the grids can be locally refined near the gap while keeping the grids logically rectangular. The resultant linear systems are solved using the MUMPS library [18], a massively parallel direct linear solver. We use meshes with a minimum of 15 points across the narrowest part of the gap and cluster grid points near the cylinder surfaces and wider gap region by stretching the constituent grids.

Applying a standard finite difference method to equations (6)–(9) is not straightforward, due to the nondifferentiable plastic dissipation term. A straightforward way of dealing with this numerical difficulty is to regularize Eq. (9) by removing the singularity at $\dot{\gamma} = 0$. This approach has been used in studies of viscoplastic flows past bluff bodies; see Refs. [19–21]. However this can yield inaccurate results, especially for lubrication-type flows or if flow stability or finite-time stoppage are of critical interest [22–24]. Instead, we use an iterative method based on the variational form of the Bingham problem, established by Duvaut and Lions [25], which forms the basis for the widely used augmented Lagrangian (AL) first proposed by Glowinski [26]. This formulation is commonly known as ALG2 and is used extensively in the literature (see Muravleva [11], Chaparian and Frigaard [27], Yu and Wachs [8] and references therein), so we do not give details here. For its solution we use the Uzawa-type algorithm of Olshanskii [28] and Muravleva and Olshanskii [29].

C. Lubrication flow in the gap

The problem shown in the inset of Fig. 1, i.e., the narrow gap between two symmetric surfaces approaching with relative speed V, has an asymptotic solution due to Balmforth [14], if the gap H is small compared to the cylinder radius R. In this section we give an overview of this solution; in Sec. III we will compare this to fully numerical solutions both in the restricted domain (inset of Fig. 1) and in the full domain. Note that this section considers a nondimensionalization of the governing equations appropriate to the gap scale; the nondimensionalization given previously in Sec. II A is appropriate for the macroscopic flow. We take x to be the coordinate across the gap and y the coordinate along the gap, consistent with the setup shown in Fig. 1.

We write $\hat{\boldsymbol{u}} \equiv (\hat{u}, \hat{v})$ and without loss of generality

$$\hat{\boldsymbol{\tau}} \equiv \begin{pmatrix} \hat{\sigma} & \hat{\psi} \\ \hat{\psi} & -\hat{\sigma} \end{pmatrix}. \tag{11}$$

Following the approach in Ref. [14], variables are scaled as

$$x = \hat{x}/\mathcal{H}, \quad y = \hat{y}/\mathcal{L}, \quad u = \hat{u}/\mathcal{U}, \quad v = \hat{v}/(\mathcal{U}/\epsilon), \quad p = \hat{p}/\mathcal{P}, \tag{12}$$

where $\epsilon \equiv \mathcal{H}/\mathcal{L}$ is a small parameter. This implies the scaled continuity equation is

$$\frac{\partial u}{\partial x} + \frac{\partial v}{\partial y} = 0. \tag{13}$$

The stress scale is chosen as $\tau = \hat{\tau}/(\epsilon\mathcal{P})$, which implies

$$\frac{\partial p}{\partial x} = \epsilon \frac{\partial \sigma}{\partial x} + \epsilon^2 \frac{\partial \psi}{\partial y}, \quad \frac{\partial p}{\partial y} = \frac{\partial \psi}{\partial x} + \epsilon \frac{\partial \sigma}{\partial y}, \tag{14}$$

so that the main force balance [to $O(\epsilon)$] is between the axial pressure gradient and transverse shear stress gradient. Strain rates are scaled by $(\mathcal{U}/\epsilon)/\mathcal{H}$, giving

$$\dot{\gamma} = \sqrt{\frac{1}{4}\left(\epsilon^2 \frac{\partial u}{\partial y} + \frac{\partial v}{\partial x}\right)^2 + \epsilon^2 \left(\frac{\partial u}{\partial x}\right)^2}. \tag{15}$$

The above scaling implies in the yielded regions

$$\tau_{ij} = \left(\frac{2\hat{\eta}\mathcal{U}}{\epsilon^2 \mathcal{P}\mathcal{H}} + \frac{\hat{\tau}_Y}{\epsilon \mathcal{P}\dot{\gamma}}\right)\dot{\gamma}_{ij}. \tag{16}$$

The velocity scale is set by the motion of the cylinders as $\mathcal{U} := V$, and therefore the pressure scale is chosen as

$$\mathcal{P} := \frac{\hat{\eta} V}{\epsilon^2 \mathcal{H}}. \tag{17}$$

We additionally fix the characteristic length and gap scales as $\mathcal{L} = R$ and $\mathcal{H} = H$, respectively. This gives the scaled constitutive equation as

$$\begin{aligned} \tau_{ij} &= \left(2 + \frac{B^*}{\dot\gamma}\right)\dot\gamma_{ij} \quad \text{if } \tau > B^*, \\ \dot\gamma_{ij} &= 0 \qquad\qquad\qquad\quad \text{if } \tau \leqslant B^*, \end{aligned} \tag{18}$$

where

$$B^* := \frac{\hat\tau_Y}{\epsilon\mathcal{P}} \tag{19}$$

is a Bingham number for the squeeze flow in the gap. Note that $B^*/\mathrm{Bn} = \epsilon^2/2$; the squeeze flow "sees" a much lower Bingham number than the macroscopic flow around the cylinders.

1. Leading-order solution

The components of the shear rate tensor are

$$\psi \equiv \dot\gamma_{xy} = \frac{1}{2}\left(\epsilon^2\frac{\partial u}{\partial y} + \frac{\partial v}{\partial x}\right), \tag{20}$$

$$\sigma \equiv \dot\gamma_{xx} = \epsilon\frac{\partial u}{\partial x}. \tag{21}$$

Therefore, discarding terms of $O(\epsilon)$, the shear rate magnitude is

$$\dot\gamma = \frac{1}{2}\left|\frac{\partial v}{\partial x}\right|, \tag{22}$$

and in the fully yielded part of the flow $\psi \gg \sigma$. Equation (18) is used to write

$$\psi = \frac{\partial v}{\partial x} + B^*\,\mathrm{sgn}\left(\frac{\partial v}{\partial x}\right), \tag{23}$$

and the main force balance reduces to

$$\frac{\partial p}{\partial x} = 0 \Rightarrow p = p(y), \quad \frac{\partial p}{\partial y} = \frac{\partial \psi}{\partial x} \Rightarrow \psi = x\frac{\partial p}{\partial y}, \tag{24}$$

the constant vanishing by symmetry, meaning that the pressure gradient is, to leading order, constant across the gap and balanced along the gap by the transverse shear stress. Exploiting the symmetry of the configuration, in the quadrant $x > 0$, $y > 0$ we must then have $v > 0$, $\frac{\partial v}{\partial x} < 0$, and so from the main force balance and constitutive law we find the velocity profile across the gap

$$\frac{\partial v}{\partial x} = x\frac{\partial p}{\partial y} + B^*, \tag{25}$$

which may be integrated to give

$$v = \begin{cases} -\frac{1}{2}\frac{\partial p}{\partial y}\left(\frac{1}{h} - x\right)\left(\frac{1}{2}h - 2X + x\right), & X < x \leqslant \frac{1}{2}h(y) \\ -\frac{1}{2}\frac{\partial p}{\partial y}\left(\frac{1}{2}h - X\right)^2, & 0 \leqslant x \leqslant X, \end{cases} \tag{26}$$

where $X \equiv B^*/|\frac{\partial p}{\partial y}|$ is the plug boundary location, and we have used a no-slip boundary condition at the cylinder surface, located at $x = \frac{1}{2}h(y)$. The continuity equation and boundary conditions imply a flow rate constraint

$$\frac{\partial}{\partial y}\int_{-\frac{1}{2}h}^{\frac{1}{2}h} v\,dx = 1, \tag{27}$$

which, when evaluated using the velocity solution, gives a cubic equation for the pressure gradient $\frac{\partial p}{\partial y}(y)$:

$$-\frac{1}{12}\frac{\partial p}{\partial y}(h+X)(h-2X)^2 = y. \tag{28}$$

It can be shown that the plug in the region $|x| < X$ undergoes $O(\epsilon)$ plastic flow, which is not present in the above asymptotic solution. This may be recovered by keeping terms $O(\epsilon)$ and is sometimes referred to as a pseudoplug; it does not change the equation for the pressure gradient to leading order [14].

For two converging cylinders the nondimensional separation distance is

$$h(y) = 1 + \frac{2}{\epsilon}(1 - \sqrt{1-y^2}), \quad 0 \leqslant |y| < 1. \tag{29}$$

We numerically evaluate Eq. (28) to compute $\frac{\partial p}{\partial y}(y)$ and thence $p(y)$, with an additional ambient pressure constraint outside the disks enforced as $p(1) = 0$. The leading-order lubrication force is then numerically computed as $2\int_0^1 p\,dy$.

D. Flow field diagnostics

In order to classify the structure of the numerically calculated flow fields we make use of an invariant measure of the velocity gradient tensor that gives an indication of the relative strength of the shear rate tensor and vorticity field [30]

$$Q = -\frac{1}{2}\frac{\partial \hat{u}_i}{\partial \hat{x}_j}\frac{\partial \hat{u}_j}{\partial \hat{x}_i} = -\frac{1}{2}\left(\hat{\dot{\gamma}}_{ij}\hat{\dot{\gamma}}_{ij} - \frac{1}{2}\hat{\boldsymbol{\omega}}^2\right), \tag{30}$$

where $\hat{\boldsymbol{\omega}}$ is the vorticity. We use the normalized form of (30)

$$\Lambda = \frac{\hat{\dot{\gamma}}_{ij}\hat{\dot{\gamma}}_{ij} - 1/2(\hat{\boldsymbol{\omega}}^2)}{\hat{\dot{\gamma}}_{ij}\hat{\dot{\gamma}}_{ij} + 1/2(\hat{\boldsymbol{\omega}}^2)}, \tag{31}$$

such that values of $\Lambda = -1,0,1$ correspond to flow dominated by rotation, shear, and strain, respectively [31].

The rate of working the fluid, $\hat{\dot{W}}$, is calculated by integrating the rate of viscous dissipation, $\hat{\Phi} = \hat{\tau}_{ij}\hat{\dot{\gamma}}_{ij}$, over a suitable control volume

$$\hat{\dot{W}}(\Omega) = \int_{\Omega - V_C} \hat{\tau}_{ij}\hat{\dot{\gamma}}_{ij}\,dV, \tag{32}$$

where V_C is the volume occupied by the cylinders. This is scaled by the force on the cylinders and the closing velocity, $\mathcal{W} = FV$, while the viscous dissipation is scaled using a characteristic energy density scale $\mathcal{E} = \eta V^2/\mathcal{H}^2$.

III. RESULTS

We investigate the squeeze flow between two infinite circular cylinders in three different cases based on the setup shown in Fig. 1. Nondimensionalization is as described in Sec. II A. The external Bingham number Bn is varied between 0 and 2000 in all cases, with the minimum separation distance kept constant at 0.01 nondimensional units (1% of the cylinder radius), resulting in a gap Bingham number B^* range of 0 to 0.1.

Two cases use the full computational domain, labeled as Ω_1 in Fig. 1, with differing far field boundary conditions. The quiescent case (meaning here that the flow is zero outside a finite yield envelope) has velocity outlets at the vertical domain boundaries, imposing an ambient pressure of

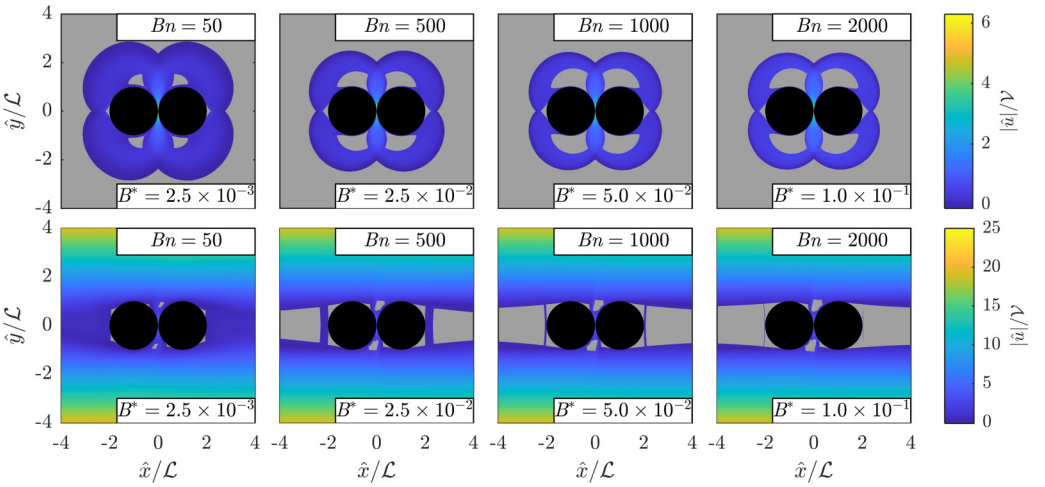

FIG. 2. Velocity magnitude plots for increasing Bn (left to right) with quiescent conditions (top row) and macroscopic shear rate $\dot{\gamma} = 5$ (bottom row).

$p = 0$. No-slip and no-penetration conditions are imposed on the horizontal domain boundaries, allowing the cylinders to be surrounded by a bounded yielded region enclosed by a yield envelope.

The shear flow case considers the same geometry as the quiescent case but with the introduction of a macroscopic flow to raise the stress above the material yield stress in the far field, thus removing the yield envelope. This is done by imposing wall velocities $\pm U_w$ on the horizontal domain boundaries, resulting in a macroscopic shear rate of $\dot{\gamma} = 5$.

Finally, we consider the reduced domain labeled as Ω_2 in Fig. 1, including only the gap between the cylinders. No-slip and no-penetration conditions are applied on the cylinder surfaces, and symmetry conditions at $x = \pm 1$ in a similar manner to Frigaard and Ryan [32] and Muravleva [11].

We begin in Sec. III A with a detailed description of the flow field kinematics for the two-cylinder system using the DNS results in the full computational domain. We then investigate the validity of the small gap approximation used to develop a leading order viscoplastic lubrication solution in Sec. III B. Following this we compare pressure profiles along the the axis of symmetry, and the resultant normal force exerted on the cylinders, to solutions from viscoplastic lubrication theory in Sec. III C. Finally, we investigate viscous dissipation in the system in Sec. III D.

A. Flow field kinematics

Figure 2 shows a binary yielded-unyielded mask in gray overlaid on color maps of the velocity magnitude for the quiescent and sheared systems, with the Bingham number increasing from left to right. The unyielded regions are identified as areas where the second invariant of the shear stress falls below the yield stress, plus some small constant which we take as 0.1% of the yield stress.

The top row in Fig. 2 corresponds to the quiescent case, where for Bn $\geqslant$ 50 classical features of moving bodies in yield stress fluids can be seen: unyielded caps on the stagnation points, unyielded plugs in the equatorial planes of the cylinders, and a yield envelope fully surrounding the two-cylinder system [19,27,33–36]. As the Bingham number increases the unyielded stagnation caps and the equatorial plugs grow while the yield envelope shrinks.

The bottom row of Fig. 2 corresponds to the shear flow case, where the background shear flow has noticeably changed the yield surface features: stagnation points have shifted, leading to two caps on the rear of the cylinders, placed symmetrically about the longitudinal axis, and one on the front of each cylinder. The equatorial plugs are no longer present, but two unattached plugs have formed

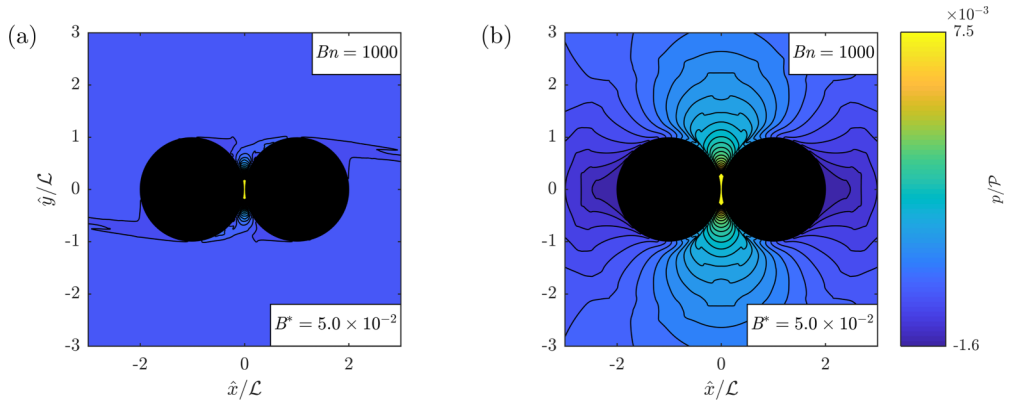

FIG. 3. Pressure contours for the two-cylinder system in macroscopic shear flow (left) and quiescent (right) with Bn = 1000.

in the gap openings, placed asymmetrically about the longitudinal axis. For Bn > 50 central plugs can be seen fore and aft of the two cylinder system.

Figure 3 show contour plots of the pressure field for a quiescent (right panel) and shear flow (left panel) case at Bn = 1000, with the contours drawn at the same levels in both panels. The quiescent case shows a pressure drop from the gap to the rear stagnation cap, with roughly equally spaced isocontours along shear layers attached to the cylinder surfaces and along the yield envelope boundary. In contrast, the shear flow case shows a rapid pressure decay along the gap with a more uniform pressure field outside of the gap.

B. Small gap approximation

In Sec. II C a lubrication approximation was constructed which has, to leading order, pressure constant across the gap. This approximation relies on the gap being small, namely, $\epsilon \ll 1$, which is satisfied at the gap center. However, since the approaching surfaces are elliptic [see Eq. (29)], this condition will be violated towards the gap exit.

We investigate the validity of this constant pressure solution by examining the ratio of the pressure at the gap center to that at the surface of the cylinder as a function of the local gap width. In the left panel of Fig. 4 we plot this gap-to-surface pressure ratio against the normalized gap width as a function of y as markers for Bn = 0−2000 ($B^* = 0-0.01$).

For all cases, the gap-to-surface pressure ratio slowly decreases towards the gap exit, but is above 0.8 until approximately $\hat{h}(\hat{y})/\mathcal{L} > 0.1$. In the Newtonian case, the pressure ratio then rapidly decreases away from the gap center, becoming negligible at the gap exit. All viscoplastic cases show similar behavior to one another (as indicated by the marker overlap in the left panel of Fig. 4). The gap-to-surface pressure ratio remains close to unity close to the gap center before slowly decreasing. Unlike for the Newtonian case, no rapid decrease is found when $\hat{h}(\hat{y})/\mathcal{L} > 0.1$, and as a result the gap-to-surface pressure remains above 0.8 further along the gap for the viscoplastic cases.

The right panel of Fig. 4 shows the pressure distributions over the entire cylinder surface, with the gap center located at $\theta = 0$ and the gap exits at $\theta = (-\pi/2, \pi/2)$, for the limiting quiescent and shear flow cases. The Newtonian surface pressure distributions of the quiescent and shear flow cases overlap, showing a peak at the gap center and a rapid decay towards the exits. For the high yield stress cases, the pressure distributions of the quiescent and shear flow cases are broadly similar, both showing a pressure peak in the gap center. However, towards the gap exit the pressure decays more slowly for the quiescent case than for the shear flow case.

In isolation, the left panel of Fig. 4 shows that the leading-order solution with constant pressure across the gap, presented in Sec. II C, is valid for only a small portion of the gap between the

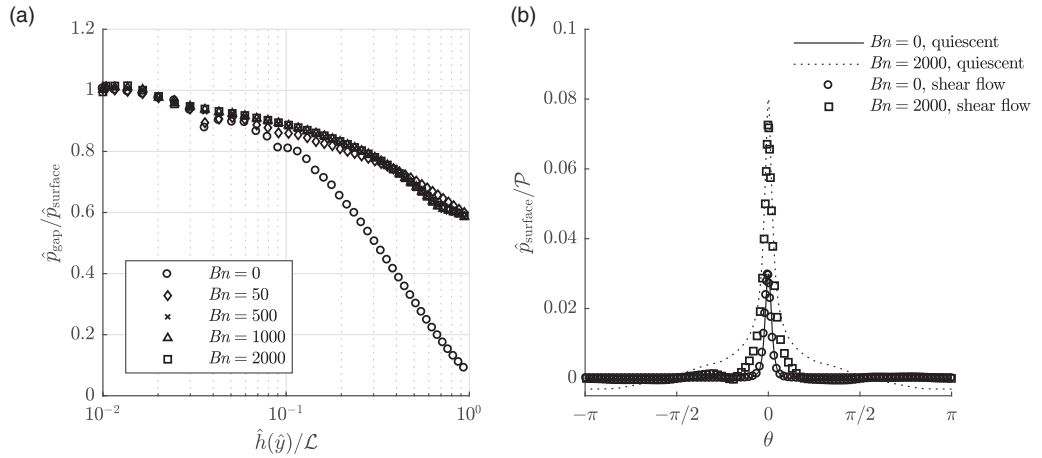

FIG. 4. Left: Ratio of center line pressure to surface pressure as a function of the local gap width for Bn = 0 (circles), 50 (diamonds), 500 (crosses), 1000 (triangles), and 2000 (squares). Right: Pressure distributions over the entire cylinder surface for the limiting Bn = 0 and Bn = 2000 quiescent flow cases as a function of angle away from the gap center.

approaching cylinders, particularly in the absence of a yield stress. However, from the surface pressure distributions in the right panel of Fig. 4 it is clear that the overwhelming contribution to the lubrication force comes from a narrow band in the gap, where the gap-to-surface pressure ratio is above 0.9 for all cases. Therefore we expect the leading-order solution to capture the lubrication force to a good approximation.

C. Pressure profiles in the gap

Figure 5 presents pressure profiles through the center of the gap, i.e., along the axis of symmetry. The direct numerical simulation (DNS) in the reduced domain gives a pressure profile in excellent agreement with the DNS of the full system in the macroscopic shear flow. Both these cases are in good agreement with the asymptotic solution from lubrication theory: peak pressures in the center of the gap match well for the full Bn range explored. At higher Bn, the DNS pressures of the shear flow and reduced domain cases remain in agreement but decay more slowly than the asymptotic solution as the gap widens up; this is where the lubrication approximation no longer holds.

The pressure profiles for the DNS of the full system in the quiescent case are markedly different to the asymptotic solution for Bn $>$ 50: higher peak pressures and slower pressure decay are evident, as is an exit pressure significantly higher than the ambient pressure (which is 0).

The relative change in peak pressure and pressure decay for increasing Bn discussed above is evident in the surface pressure distribution shown in Fig. 4. Moreover, it is evident that the pressure contribution outside of the nominal gap region is negligible. Note that for Bn = 2000 the pressure profiles look somewhat similar in magnitude between the quiescent and sheared cases. In fact their integrals differ by about a factor of two, implying a factor of two difference in the repulsive force; this is discussed next.

Figure 6 presents stacked area plots of the total drag force exerted on a cylinder, decomposed into pressure and viscous contributions. From the left panel it is clear that the force on the cylinders in quiescent fluid is dramatically underestimated when the lubrication flow in the gap is considered in isolation. Both viscous and pressure contributions increase with Bn, but the viscous contribution remains small compared to that of the pressure. Discounting the viscous friction, the pressure alone—which remains localized to the gap—causes a more than twofold increase in the drag force over the predictions from lubrication theory. However, when a macroscopic shear flow is added (the right

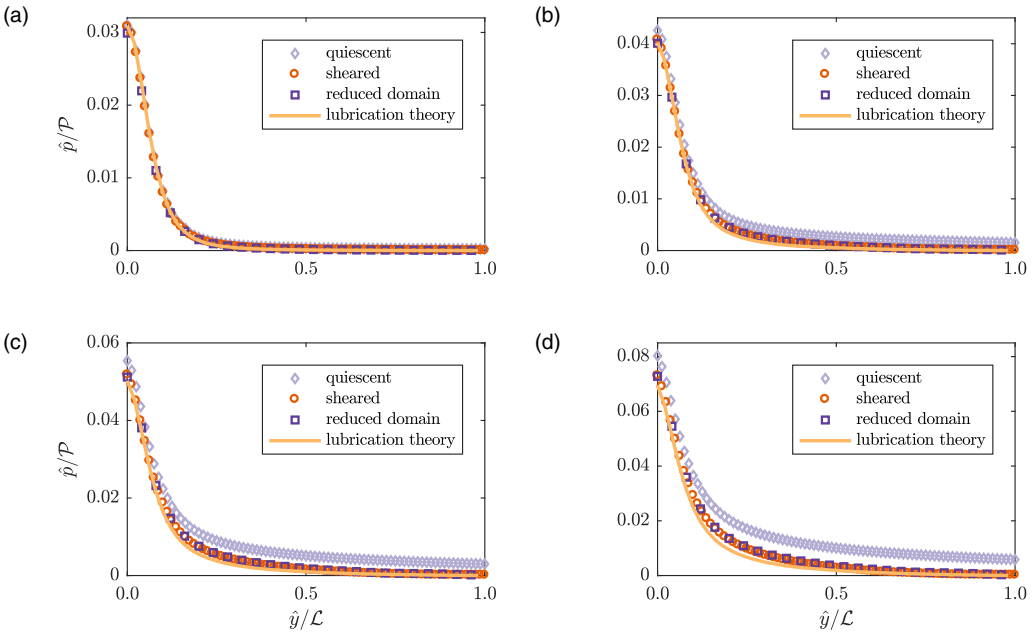

FIG. 5. Pressure profile along the gap center line for quiescent (diamonds), sheared (circles), and reduced domain (square) systems with viscoplastic lubrication solution overlayed (solid line) with Bn = 50, 500, 1000, 2000 in plots (a) through (d), respectively.

panel in Fig. 6), the total drag force is close to the asymptotic solution. This mirrors the trend found in the pressure profiles in Fig. 5.

Figure 7 shows local shear rates, $\dot{\gamma}_{\text{local}}$, for both the sheared and quiescent cases for the full range of Bn. We define the local shear rate as an average over a $H \times 2H$ area in the center of the gap. The dramatic increase in pressure and drag force is not reflected in the local shear rate: the local shear rates in the quiescent and sheared cases remain in close agreement throughout the Bn range explored. From this we can conclude that the macroscopic flow does not affect the velocity field in the gap.

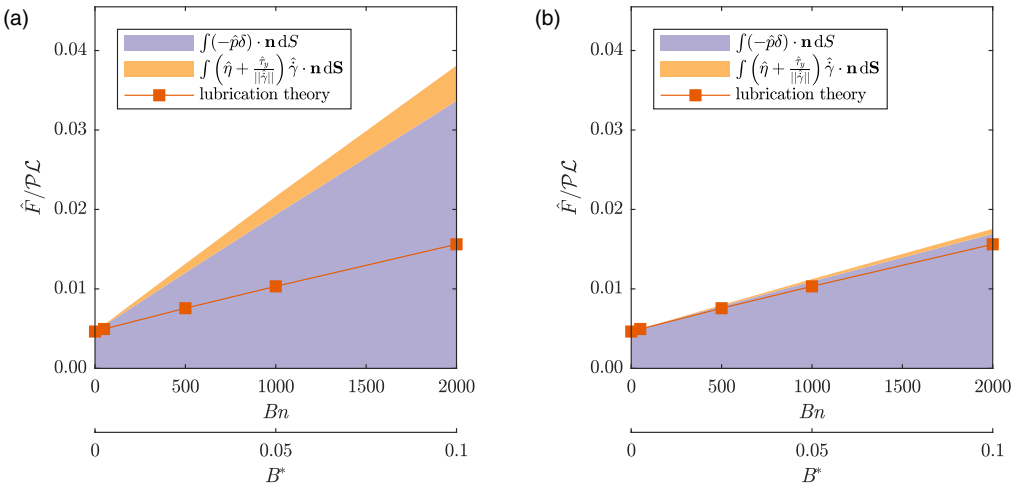

FIG. 6. Stacked area plots of the total drag force on a cylinder as a function of Bn for (a) quiescent and (b) shear flow background conditions. Overlaid are the predictions from viscoplastic lubrication theory (squares).

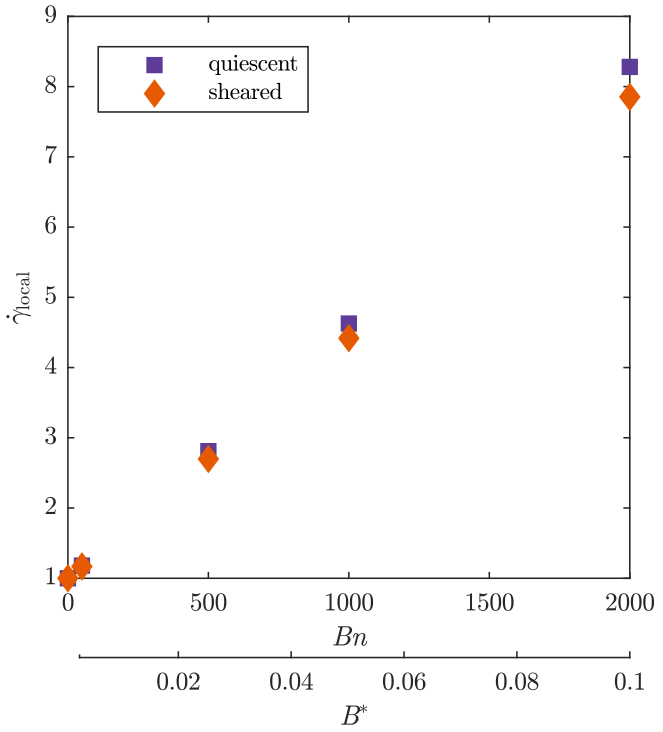

FIG. 7. Local shear rates in the gap center for quiescent (squares) and sheared (diamonds) systems for Bn = 0, 50, 500, 1000, 2000.

The above computations were also performed with a macroscopic shear rate one order of magnitude higher, showing no appreciable differences in the pressure and force results discussed above.

D. Viscous dissipation

The left panel of Fig. 8 shows a color map of $\log_{10}(\dot{\gamma})$ in a quiescent case, while the right panel shows a contour plot of the normalized second invariant of the velocity gradient tensor, indicating where the fluid is irrotational (red), rotational (blue), and being sheared (green), with the yield surface

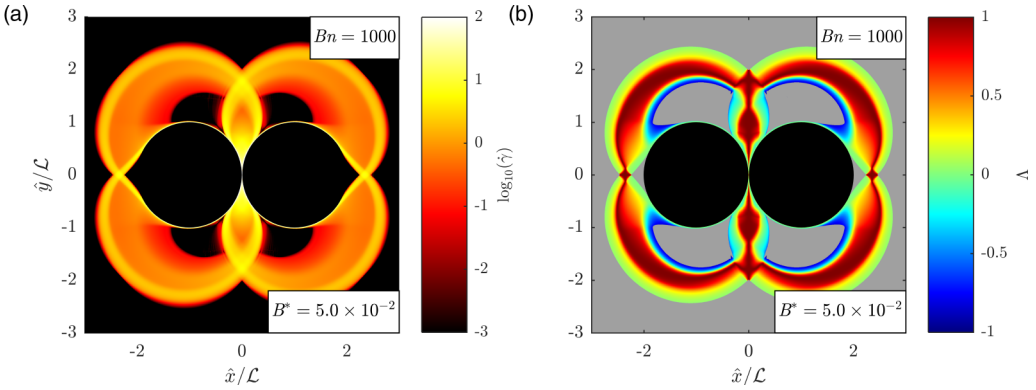

FIG. 8. (a) Color map of $\log_{10}(\dot{\gamma})$ and (b) normalized second invariants of the velocity gradient tensor with unyielded areas masked in gray with Bn = 1000 (quiescent case).

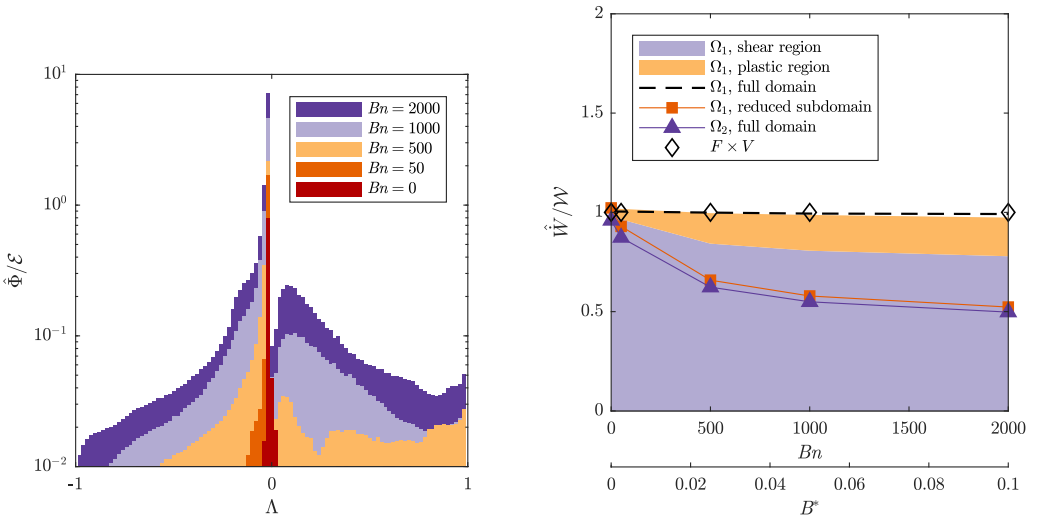

FIG. 9. Left: rate of mechanical dissipation per unit Λ. Right: stacked area plot showing the rate of work done by viscous dissipation in the shear and plastic regions, scaled by $\mathcal{W} = FV$, with markers indicating the power required to move the cylinders with the approach velocity (diamonds), the total viscous dissipation in the system (dashed line), the viscous dissipation in the gap region of the full system (squares), and the total viscous dissipation in the reduced system (triangles).

overlaid. As expected, the plugs either side of the cylinders undergo rigid body rotation. Strain rates are highest in the thin shear layers along the cylinder surface, along the yield envelope wall, and surrounding the jet of fluid squeezed out of the gap. Strain-dominated regions are found in the core of the fluid jet squeezed out of the gap, and in the regions between the rotating plugs and the yield envelope. The strain rate in these plastic flow regions is orders of magnitude lower than in the adjacent shear layers.

We turn now to the energy dissipation in the fluid. The left panel of Fig. 9 shows the rate of mechanical dissipation as a function of the topology parameter Λ. As would be expected, no dissipation occurs in the regions undergoing rigid body rotation ($\Lambda = -1$). Some dissipation is evident in the irrotational regions ($\Lambda = 1$) at high Bingham numbers, and this is attributed to pseudoplug regions where the flow is held close to the yield stress [37].

In all cases the dissipation is highest in regions of shear, peaking at $\Lambda = 0$. While the rate of mechanical dissipation decreases monotonically as the flow becomes rotationally dominated, for $\mathrm{Bn} > 0$ as the flow becomes dominated by strain there exists a second, small peak in dissipation which decays slowly as Λ approaches 1.

The right panel of Fig. 9 shows the rate of work done on the fluid in different regions and flow structures for the full and reduced systems, as well as the power required to move the cylinders with the set approach velocity. Shear regions and plastic regions have been defined as areas where $-1/3 \leqslant \Lambda \leqslant 1/3$ and $\Lambda > 1/3$, respectively [31]. While the dissipation in plastic flow is small compared to that in shear flow, it still forms a significant source of viscous dissipation outside of the gap area due to the size of the plastic flow regions (see Fig. 8). Finally, the rate of work done in the gap region is very similar for both the full (Ω_1) and reduced (Ω_2) domains. This shows that the excess drag force on the cylinders in the full domain compared to lubrication theory [Fig. 6(a)] arises from energy dissipation external to the gap.

IV. CONCLUSIONS

In this paper we have presented results on the squeeze flow between two infinite circular cylinders in a Bingham fluid, which we use as a simple model for the flow of noncolloidal particles in a

viscoplastic fluid. Understanding this flow is essential to building models of the large-scale flow of such suspensions. Although the calculations presented here have been two-dimensional, we expect similar phenomena will occur in three dimensions (where the particles would be spheres).

In Sec. III we presented results from three numerical experiments: two modeling the approaching cylinders within a quiescent and a sheared fluid, and one modeling just the gap between the approaching cylinders, removing any external influence. We showed that unlike for a Newtonian fluid, the macroscopic flow external to the gap has a large effect on the lubrication forces felt by two cylinders in near contact. In a quiescent Bingham fluid, the lubrication forces were approximately double those predicted by viscoplastic lubrication theory, but were still caused primarily by the localized high lubrication pressure in the gap, as for a Newtonian fluid. The high lubrication pressure compared to theory is due to the enclosing yield envelope which forms around the two particle system and causes a recirculating flow, introducing significant viscous dissipation into the system. Most of the extra viscous dissipation occurs in shear layers along the cylinder surface and yield envelope walls, although at high Bingham numbers the contribution from plastic flow regions near the yield envelope becomes appreciable.

Introducing a macroscopic shear flow or modeling just the gap area between the cylinders gave nearly identical results and agreed closely with the predictions from lubrication theory. We conclude that the background shear flow acts to eliminate the yield envelope in the macroscopic flow around the particles. This in turn removes the recirculating flow and complex flow structures, where large sources of viscous dissipation in the quiescent case appear, and hence lowers the lubrication pressure and resulting lubrication force. The resulting pressure profiles in the gap are well described by lubrication theory local to the gap. The results indicate that the macroscopic shear rate does not appreciably affect the velocity field in the narrow gap region. This conclusion is insensitive to the exact macroscopic shear rate used, provided the yield envelope is removed.

The above implies that lubrication force models using an effective viscosity based on the local shear rate (such as the approach used for shear-thinning fluids in Vázquez-Quesada *et al.* [38]) may not be accurate for viscoplastic fluids. Instead, we suggest the use of subgrid-scale lubrication force models based on viscoplastic lubrication theory, with the understanding that they may become invalid in regions without a macroscopic stress above the yield stress, i.e., where particles become confined by their own yield envelopes. This will allow for a large range of validity, for example, in simulations of the type considered in Refs. [38,39] among others, where a dense suspension is subject to shear, and a subgrid-scale lubrication force model is needed due to the close particle-particle approaches. However, in other cases, for example, dilute particulate suspensions sedimenting in a quiescent fluid, we have shown in this paper that a subgrid-scale lubrication force model based solely on lubrication theory in the gap may not be appropriate. Until a more sophisticated subgrid-scale model is developed, the only current option is DNS computations with sufficiently high resolution in the interparticle gaps.

ACKNOWLEDGMENTS

A.R.K. acknowledges financial support from the EPSRC Centre for Doctoral Training in Computational Methods for Materials Science under Grant No. EP/L015552/1. This work was supported by the Schlumberger Gould Research Centre.

[1] G. Ovarlez, F. Mahaut, S. Deboeuf, N. Lenoir, S. Hormozi, and X. Chateau, Flows of suspensions of particles in yield stress fluids, J. Rheol. **59**, 1449 (2015).

[2] M. Stimson and G. B. Jeffery, The motion of two spheres in a viscous fluid, Proc. R. Soc. London A **111**, 110 (1926).

[3] A. Umemura, Matched-asymptotic analysis of low-Reynolds-number flow past two equal circular cylinders, J. Fluid Mech. **121**, 345 (1982).

[4] B. T. Liu, S. J. Muller, and M. M. Denn, Interactions of two rigid spheres translating collinearly in creeping flow in a Bingham material, J. Non-Newtonian Fluid Mech. **113**, 49 (2003).
[5] M. R. Horsley, R. R. Horsley, K. C. Wilson, and R. L. Jones, Non-Newtonian effects on fall velocities of pairs of vertically aligned spheres, J. Non-Newtonian Fluid Mech. **124**, 147 (2004).
[6] P. Jie and Z. Ke-Qin, Drag force of interacting coaxial spheres in viscoplastic fluids, J. Non-Newtonian Fluid Mech. **135**, 83 (2006).
[7] O. Merkak, L. Jossic, and A. Magnin, Spheres and interactions between spheres moving at very low velocities in a yield stress fluid, J. Non-Newtonian Fluid Mech. **133**, 99 (2006).
[8] Z. Yu and A. Wachs, A fictitious domain method for dynamic simulation of particle sedimentation in Bingham fluids, J. Non-Newtonian Fluid Mech. **145**, 78 (2007).
[9] D. L. Tokpavi, P. Jay, and A. Magnin, Interaction between two circular cylinders in slow flow of Bingham viscoplastic fluid, J. Non-Newtonian Fluid Mech. **157**, 175 (2009).
[10] L. Jossic and A. Magnin, Drag of an isolated cylinder and interactions between two cylinders in yield stress fluids, J. Non-Newtonian Fluid Mech. **164**, 9 (2009).
[11] L. Muravleva, Squeeze plane flow of viscoplastic Bingham material, J. Non-Newtonian Fluid Mech. **220**, 148 (2015).
[12] D. N. Smyrnaios and J. A. Tsamopoulos, Squeeze flow of Bingham plastics, J. Non-Newtonian Fluid Mech. **100**, 165 (2001).
[13] L. Muravleva, Axisymmetric squeeze flow of a viscoplastic Bingham medium, J. Non-Newtonian Fluid Mech. **249**, 97 (2017).
[14] N. J. Balmforth, R. Craster, D. Hewitt, S. Hormozi, and A. Maleki, Viscoplastic boundary layers, J. Fluid Mech. **813**, 929 (2017).
[15] G. S. Chesshire and W. D. Henshaw, Composite overlapping meshes for the solution of partial differential equations, J. Comput. Phys. **90**, 1 (1990).
[16] W. D. Henshaw, Ogen: An overlapping grid generator for Overture, Research Report UCRL-MA-132237 (Lawrence Livermore National Laboratory, 1998).
[17] A. R. Koblitz, S. Lovett, N. Nikiforakis, and W. D. Henshaw, Direct numerical simulation of particulate flows with an overset grid method, J. Comput. Phys. **343**, 414 (2017).
[18] P. R. Amestoy, I. S. Duff, J.-Y. L'Excellent, and J. Koster, A fully asynchronous multifrontal solver using distributed dynamic scheduling, SIAM J. Matrix Anal. Appl. **23**, 15 (2001).
[19] D. L. Tokpavi, A. Magnin, and P. Jay, Very slow flow of Bingham viscoplastic fluid around a circular cylinder, J. Non-Newtonian Fluid Mech. **154**, 65 (2008).
[20] T. Zisis and E. Mitsoulis, Viscoplastic flow around a cylinder kept between parallel plates, J. Non-Newtonian Fluid Mech. **105**, 1 (2002).
[21] S. Mossaz, P. Jay, and A. Magnin, Criteria for the appearance of recirculating and non-stationary regimes behind in a viscoplastic fluid, J. Non-Newtonian Fluid Mech. **165**, 1525 (2010).
[22] I. A. Frigaard and C. Nouar, On the usage of viscosity regularisation methods for visco-plastic fluid flow computation, J. Non-Newtonian Fluid Mech. **127**, 1 (2005).
[23] A. Putz, I. A. Frigaard, and D. M. Martinez, On the lubrication paradox and the use of regularisation methods for lubrication flows, J. Non-Newtonian Fluid Mech. **163**, 62 (2009).
[24] A. Wachs and I. A. Frigaard, Particle settling in yield stress fluids: Limiting time, distance and applications, J. Non-Newtonian Fluid Mech. **238**, 189 (2016).
[25] G. Duvaut and J. L. Lions, *Les Inéquations en Mécanique et en Physique* (Dunod, 1972).
[26] R. Glowinski, *Numerical Methods for Non-Linear Variational Problems* (Springer, 1984).
[27] E. Chaparian and I. A. Frigaard, Yield limit analysis of particles motion in a yield-stress fluid, J. Fluid Mech. **819**, 311 (2017).
[28] M A. Olshanskii, Analysis of semi-staggered finite-difference method with application to Bingham flows, Comput. Methods Appl. Mech. Eng. **198**, 975 (2009).
[29] E. A. Muravleva and M. A. Olshanskii, Two finite-difference schemes for calculation of Bingham fluid flows in a cavity, Russ. J. Numer. Anal. Math. Model. **23**, 615 (2008).
[30] P. A. Davidson, *Turbulence: An Introduction for Scientists and Engineers* (Oxford University Press, 2004).

[31] S. De, J. A. M. Kuipers, E. A. J. F. Peters, and J. T. Padding, Viscoelastic flow simulations in model porous media, Phys. Rev. Fluids **2**, 053303 (2017).
[32] I. A. Frigaard and D. P. Ryan, Flow of a visco-plastic fluid in a channel of slowly varying width, J. Non-Newtonian Fluid Mech. **123**, 67 (2004).
[33] A. Putz and I. A. Frigaard, Creeping flow around particles in a Bingham fluid, J. Non-Newtonian Fluid Mech. **165**, 263 (2010).
[34] A. N. Beris, J. H. Tsamopoulos, R. C. Armstrong, and R. A. Brown, Creeping motion of a sphere through a Bingham plastic, J. Fluid Mech. **158**, 219 (1985).
[35] R. W. Ansley and T. N. Smith, Motion of spherical particles in a Bingham plastic, AIChE **13**, 1193 (1967).
[36] K. Adachi and N. Yoshioka, On creeping flow of a visco-plastic fluid past a circular cylinder, Chem. Eng. Sci. **28**, 215 (1973).
[37] I. C. Walton and S. H. Bittleston, The axial flow of a Bingham plastic in a narrow eccentric annulus, J. Fluid Mech. **222**, 39 (1991).
[38] A. Vázquez-Quesada, R. I. Tanner, and M. Ellero, Shear Thinning of Noncolloidal Suspensions, Phys. Rev. Lett. **117**, 108001 (2016).
[39] X. Bian and M. Ellero, A splitting integration scheme for the SPH simulation of concentrated particle suspensions, Comput. Phys. Commun. **185**, 53 (2014).